



Article

In Vitro Cytotoxicity Assessment of Green Synthesized CuO: NiO Nanocomposites Against Human Prostate Cancer Cells

Jawad N. K. Makassees¹, Ali K. Hattab², Ali A. Fayyadh³

1. Ministry of Education, General Directorate of Wasit Education, Wasit, Iraq.

2. Department of Physics, College of Science, University of Wasit, Wasit, Iraq.

3. Ministry of Education, General Directorate of Wasit Education, Wasit, Iraq.

* Correspondence: -

Abstract: In vitro cytotoxic evaluation of CuO:NiO nanocomposites synthesized using two phytochemical routes employing *Cinnamomum cassia* and *Mentha* plant extracts against human prostate cancer cell line (DU145) and human foreskin fibroblast (HFF) were investigated in this study. Also, comprehensive characterization to study the structural and morphological analyses using XRD, FTIR, FESEM, and EDX techniques. According to XRD, *Cinnamomum cassia*-mediated and *Mentha*-mediated nanocomposites formed crystalline phases with 25.14 nm and 20.27 nm crystallite sizes, respectively. FESEM observations revealed that the particles in *Cinnamomum cassia*-mediated nanocomposites are clustered and spherical, while in *Mentha*-mediated nanocomposites, they are more uniform in size and less likely to cluster. The elemental analysis of EDX found Cu, Ni, and O in both nanocomposites, but the *Cinnamomum cassia* had a higher amount of Cu (33.69%) and Ni (28.00%) than those prepared using *Mentha* (Cu: 21.87% and Ni: 22.10%). Both types of nanocomposites were found to have low toxicity toward the normal HFF cells, but were more selective cytotoxicity against the DU145 cancer cells. The anticancer effect of *Cinnamomum cassia*-based nanocomposites show greater ($IC_{50} = 864.41 \mu\text{g/mL}$) than that of *Mentha*-based nanocomposites ($IC_{50} = 920.28 \mu\text{g/mL}$). The morphological analysis of cells after cancer therapy showed that cell changes indicating apoptosis were more pronounced between 400-800 $\mu\text{g/mL}$. Based on the results, producing CuO:NiO nanocomposites with useful applications in cancer therapy can be achieved with green synthesis by using plant extracts, since the type of compounds in the extract greatly influences both the properties and the biological activity of the final nanocomposites.

Keywords: CuO:NiO nanocomposite, green synthesis, cytotoxicity, crystallite, prostate cancer.

Citation: Makassees, J. N. K., Hattab, A. K & Fayyadh, A. A. In Vitro Cytotoxicity Assessment of Green Synthesized CuO: NiO Nanocomposites Against Human Prostate Cancer Cells. Vital Annex: International Journal of Novel Research in Advanced Sciences 2025, 4(6), 195-208.

Received: 10th Mar 2025Revised: 16th Apr 2025Accepted: 24th May 2025Published: 23th Jun 2025

Copyright: © 2025 by the authors. Submitted for open access publication under the terms and conditions of the Creative Commons Attribution (CC BY) license (<https://creativecommons.org/licenses/by/4.0/>)

1. Introduction

Nanotechnology has allowed for the development of new nanomaterials in medicine that safely and effectively treat cancer, while other treatments may not. Many researchers are attracted to metal oxide nanocomposites because they have high surface areas, several morphologies and strong catalytic activity. Among nanostructures, copper oxide (CuO) and nickel oxide (NiO) are highly regarded in anticancer treatment because they kill cancerous cells with the help of reactive oxygen species (ROS), resulting in oxidative stress. Generally, synthesising metal oxide nanoparticles involves hazardous materials and consumes a lot of energy which worries many people about the environment and safety for living organisms. Different from the previous method, green synthesis involving plant extracts is now preferred as a safe and eco-friendly choice, due to the reducing and stabilizing powers of plant-based chemicals. The Phyto molecules not only decrease metal ions in the solution but also act as agents that cap the nanostructures and shape their appearance, size and stability in water. Furthermore, the bioactive compounds

embedded in plant extracts can impart additional biological functionalities, potentially enhancing the therapeutic efficacy of the resulting nanocomposites through synergistic effects. The characteristics and activities of the nanoparticles are significantly impacted by the selection of plant extracts. *Cinnamomum cassia* extract plant contains chemicals like cinnamaldehyde, eugenol and polyphenols that have proven effects against free radicals, antimicrobial, and anticancer properties. These compounds possess functional groups capable of reducing metal ions and stabilizing nanoparticles through surface interactions. Similarly, *Mentha* plant extract also contains menthol, menthone, rosmarinic acid and flavonoids with different biological properties and they can be efficiently used in nanoparticle synthesis. Plant extracts play a major role in determining how the final nanoparticles will act physically and with biological materials. Bioactive chemicals including cinnamaldehyde, eugenol and different polyphenols with recognized antioxidant, antimicrobial and anticancer benefits are present in *Cinnamomum cassia*. They are designed to act on metal ions by reducing them and hold the nanoparticle surface stable via interactions. In addition, *Mentha* species are full of menthol, menthone, rosmarinic acid and flavonoids that have various biological activities and are useful for making nanoparticles. Cancer nanotechnology is challenged by the need to selectively kill malignant cells without harming healthy ones. Because prostate cancer is the second most frequently diagnosed cancer in men, it should be a main focus in developing new treatment strategies. Since DU145 cells are from brain metastasis and act like androgen-independent prostate cancer, they are commonly used to study the efficacy of new anticancer substances in the laboratory. Metal oxide nanoparticles use a range of pathways to harm cells, including causing ROS, dysfunction of the mitochondria, changes in DNA and leaking of cell contents. Cancer cells commonly react more strongly to agents that increase oxidative stress than healthy cells do. Having this differential susceptibility creates an opportunity for making cancer-selective medicines at the nanoscale. Also, a special effect called EPR in tumor tissues helps nanoparticles to concentrate in those areas which makes them better able to target and destroy cancer cells. Still, using metal oxide nanoparticles in clinics is hindered by some main concerns about toxicity, where they go in the body and how fast they are cleared. To resolve these points, green synthesis looks to minimize dangerous chemicals and incorporate gentle, biological coating agents that can modify how nanoparticles interact with living things. As well, learning how synthesis settings and plant chemicals influence nanoparticle properties is necessary for developing methods that can be repeated. This work seeks to fabricate CuO:NiO nanocomposites using extracts from *Cinnamomum cassia* and *Mentha* and carefully analyze their features with XRD, FTIR, FESEM and EDX. The research checks the ability of these nanomedicines to destroy prostate cancer cells (DU145) compared to normal cells (HFF) in the laboratory. This study helps advance the development of metal oxide nanocomposites in cancer treatment by understanding the relationships among how they are produced, what they look like and their activities in the body.

2. Materials and Methods

Materials

Copper (II) nitrate trihydrate ($\text{Cu}(\text{NO}_3)_2 \cdot 3\text{H}_2\text{O}$, 99.5%) and nickel (II) nitrate hexahydrate ($\text{Ni}(\text{NO}_3)_2 \cdot 6\text{H}_2\text{O}$, 98%) were the metals used in the making of CuO:NiO nanocomposites. *Cinnamomum cassia* bark and fresh *Mentha* leaves were all thoroughly cleaned in deionized water, air-dried at room temperature for three days, minced to fine particles and transferred to airtight containers at 4°C until used. Use RPMI-1640 medium with 10% fetal bovine serum (FBS), 1% penicillin-streptomycin solution, 0.25% trypsin-EDTA solution, sterile phosphate-buffered saline (PBS, pH 7.4), human prostate cancer cell line (DU145) and human foreskin fibroblast (HFF) obtained from American Type Culture Collection (ATCC, Manassas, VA, USA), 3-(4,5-dimethyl.

Methods

Cell culture

Cells from the human prostate cancer cell line (DU145) and human foreskin fibroblast (HFF) were obtained from the American Type Culture Collection (ATCC, Manassas, VA,

USA). RPMI-1640 medium combined with 10% fetal bovine serum (FBS) and 1% penicillin-streptomycin solution served as the growth medium for cells during culture. The cultures received incubation at 37°C under atmospheric conditions with 5% CO₂ levels along with high humidity. The subculture occurred whenever cells achieved 80-85% confluence by using a trypsin-EDTA solution at 0.25%.

Preparation of nanocomposite suspensions

Nanocomposite samples of CuO: NiO were dispersed in sterile phosphate-buffered saline (PBS, pH 7.4) for 15 minutes while using sonication at a pulse mode with 5 s of operation followed by 3 s intervals to achieve uniform dispersion. Culture medium served to dilute stock suspensions until concentrations reached 25, 50, 100, 200, 400, and 800 µg/mL for cytotoxicity testing.

MTT assay

Cell viability measurement occurred through MTT assay. The cells developed from DU145 and HFF were seeded at 1×10^4 cells/well density within 96-well plates before allowing 24-hour adherence. The cell incubation duration at 48 h utilized fresh medium containing different copper oxide nanocomposite concentrations from 25 to 800 µg/mL. The MTT solution (5 mg/mL in PBS) at 20 µL volume was added to each well before a 4-hour incubation at 37°C. The analyzed wavelength for measuring formazan crystallite absorbance corresponded to 570 nm through a BioTek Instruments microplate reader (operations in Winooski, VT, USA) with 630 nm as its reference wavelength. The formazan crystals were solubilized using 100 µL DMSO. The calculation of cell viability required the given formula:

$$\text{Cell viability} = \left(\frac{\text{Absorbance of treated cells}}{\text{Absorbance of control cells}} \right) \times 100 \% \dots \dots \dots 1$$

The half-maximal inhibitory concentration (IC₅₀) values emerged through GraphPad Prism (software version 8.0, GraphPad Software, San Diego, CA, USA) from dose-response curve graphs.

Morphological Analysis

The microscopic changes in cells became visible through phase-contrast microscopy after a 48-hour exposure period with different concentrations of nanocomposites. The study team recorded sample photographs to evaluate how different drug amounts affected cell structural appearance and population density.

Characterization Techniques

Multiple advanced analytical techniques were used to properly study the CuO:NiO nanocomposites. Analyzing the structure involved use of a D8 advance X-ray diffractometer (Bruker) under monochromated Cu K α radiation ($\lambda = 1.54060 \text{ \AA}$) operating at 50 kV and 40 mA. The X-ray diffractometer collected diffraction data between 20° to 90° by using a 0.01° step size and 1.5 s time-per-step duration which supported precise crystallite phase detection and crystal size assessment using the Scherrer equation. The analysis of chemical bonding and functional groups used an FT-IR spectra collection process performed by a Jasco FT/IR-4600 spectrometer that incorporated a DLATGS detector. Direct analysis of the powder became possible through the utilization of the DRIFTS sampling technique during measurements within the mid-IR region (4000–400 cm⁻¹). Successful formation of metal oxide was observed through the spectra which showed distinct peaks from Cu–O and Ni–O stretching vibrations. An FESEM-type Hitachi SU8220 was used to perform imaging at 20 kV with an accelerating voltage. The instrument allowed users to analyze surface features together with nanoparticle distribution patterns and dimensions at high magnification. Additional elemental analysis procedures took place with the help of an EDS detector developed by EDAX. The laboratory results obtained from quantitative energy-dispersive X-ray spectroscopy demonstrated the existence of Cu, Ni, and O elements while producing stoichiometric and homogeneous information about the synthesized CuO:NiO nanocomposites.

3. Results and Discussion

X-ray diffraction (XRD) analysis provided investigations into the crystal structures that developed during synthesis of the CuO:NiO nanocomposite. X-ray diffraction

functions based on Bragg's law that establishes a relation between interplanar spacing and diffraction angle.

$$n\lambda = 2d \sin \theta \dots\dots\dots 2$$

The X-ray diffraction pattern depends on four main elements which include the diffraction order (n) and X-ray wavelength (λ) as well as the crystal lattice plane spacing (d) and X-ray beam incident angle (θ). The relation functions as a fundamental basis for crystal structure discovery in crystalline substances [Click or tap here to enter text..](#) The assessment of crystallite size (D) relied on the Scherrer equation.

$$D = (k\lambda)/(\beta \cos \theta) \dots\dots\dots 3$$

The XRD peak analysis relies on K as the shape factor with a value of 0.94 while λ stands for the $\text{CuK}\alpha$ radiation wavelength (0.154060 nm) and β represents the full width at half maximum (FWHM) which measures peak width in radians and θ stands for Bragg diffraction angle. The XRD patterns in Figs. 1 and 2 display distinct peaks attributed to monoclinic CuO (COD entry: 96-901-5823/96-901-6106) together with cubic NiO (COD entry: 96-432-0506) phases. For both *Cinnamomum*-mediated and *Mentha*-mediated samples the strongest XRD peaks appeared at 36.87° , 38.54° and 43.00° and at 37.03° , 38.70° and 43.01° respectively. The (111) and (200) crystal plane peaks alongside peak (111) indicate that pure crystalline nanocomposite substances have formed without detectable impurity phases. Standard d-spacing values demonstrate close correspondence to experimental measurements while minor deviations may stem from both lattice strain and size effects caused by the biomolecules occurring in plant extracts. The d-spacings of the *Cinnamomum*-mediated sample showed experimental measurements at 2.4349 Å, 2.3339 Å, and 2.1018 Å that closely matched standard values at 2.4251 Å, 2.3392 Å, and 2.1005 Å. The *Mentha*-mediated sample obtained d-spacing values at 2.4257 Å, 2.3240 Å and 2.1014 Å which matched closely with the standard values of 2.4254 Å, 2.3207 Å and 2.1003 Å.

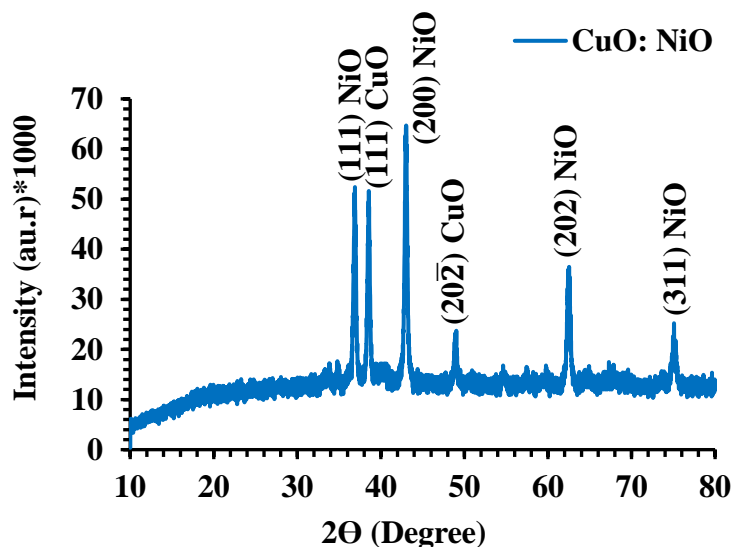


Figure 1. XRD pattern of *Cinnamomum cassia*-mediated CuO:NiO nanocomposite.

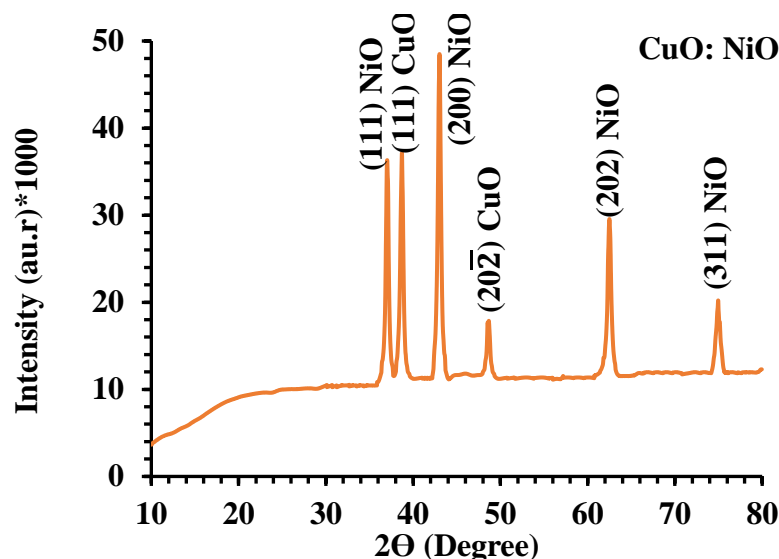


Figure 2. XRD pattern of *Mentha*-mediated CuO:NiO nanocomposite.

The crystallite sizes determined by Scherrer equation analysis indicated substantial differences in the production methods. *Cinnamomum cassia*-mediated nanocomposite synthesized larger crystallite dimensions (25.14 nm) than *Mentha*-mediated nanocomposite with dimensions (20.27 nm). Analysis shows that different growth mechanisms controlled by plant extract phytochemical formulations influence the crystallite size variations [1]. The *Cinnamomum cassia*-mediated sample formed crystallites measuring 25.75, 25.84, and 23.82 nanometers in size for its three principal peaks and the crystallites of the *Mentha*-mediated sample reduced to 20.99, 20.48, and 19.33 nanometers. The crystallite sizes decreased in the *Mentha*-mediated sample because its high polyphenols and flavonoids content effectively limited nanoparticle growth at nucleation and crystallization stages [2]. The analysis of the nanocomposites demonstrates that plant extract selection directly affects crystallographic properties in the final structures. The *Mentha* extract demonstrates superior capping properties such that crystallite sizes remain smaller and surface area-to-volume ratios become higher. Surface reactivity functions as a key factor in catalytic processes and sensing applications and this characteristic turns out beneficial due to its presence [3]. Both samples show identical d-spacing patterns between their experimental and standard data thus revealing stoichiometric formation of CuO and NiO crystal phases with small lattice deformation even though synthesis methods were different. The slight peak position and intensity variations indicate that defect concentration and strain differences along with crystallinity changes result from the specific biomolecules within each plant extract [4]. The FTIR spectrum of *Cinnamomum cassia*-mediated CuO nanocomposite (Fig. 3) displays numerous distinctive absorption bands which reveal information about its molecular framework and surface modifications. The main spectral bands within this spectrum originate simultaneously from both metal oxide material and organic compounds found in plant extract materials. The O-H stretching vibrations which appear as a broad absorption band from 3200-3600 cm^{-1} demonstrate hydroxyl group presence together with water molecules bound to nanoparticle surfaces [5]. Absorption bands between 2850-2950 cm^{-1} indicate C-H stretching from methyl and methylene groups which exist within the organic *Cinnamomum cassia* compounds especially cinnamaldehyde and eugenol [6]. The absorption bands between 1600-1700 cm^{-1} detect C=O stretching vibrations from carbonyl compounds like aldehydes and ketones and the peaks within 1450-1650 cm^{-1} signify C=C stretching vibrations of aromatic rings [7]. The appearance of bands through spectrum analysis confirms how polyphenolic compounds from the *Cinnamomum cassia* extract bind onto surface areas of nanoparticles. The fingerprint region (1400-400 cm^{-1}) reveals metal-oxygen vibrational modes that produce bands between 500-700 cm^{-1} which correspond to Cu-O and Ni-O stretchings. The formation of CuO and NiO crystalline phases becomes validated by the appearance of these bands [8]. The interaction between plant-derived

organic compounds and metal oxide surface is confirmed through the appearance of C-O stretching vibrations between 1000-1100 cm^{-1} [9].

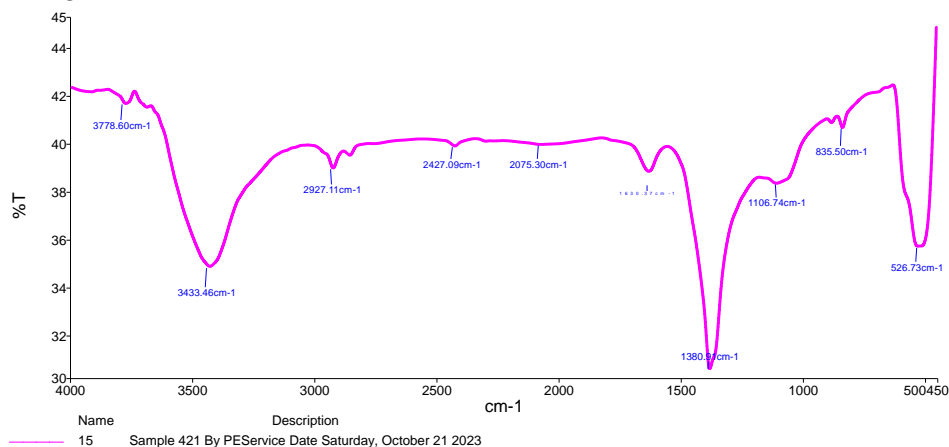


Figure 3. FTIR pattern of *Cinnamomum cassia*-mediated CuO:NiO nanocomposite.

The FTIR spectrum of *Mentha*-CuO nanocomposites displays different absorption patterns than *Cinnamomum cassia*-CuO nanocomposites which indicates the distinct phytochemical features of *Mentha*-based extract in Fig. 4. Hydroxyl groups show their appearance as a broad band between 3200-3600 cm^{-1} in the FTIR spectrum just like the *Cinnamomum cassia*-mediated sample. The intensity together with breadth of this band differs from the others demonstrating various degrees of hydroxylation and hydrogen bonding occurrence as reported in [10]. The C-H stretching vibrations at 2850-2950 cm^{-1} present different intensity levels in the *mentha* extract compared to those of the *Cinnamomum cassia*-mediated control sample which demonstrates their unique aliphatic content composition [11].

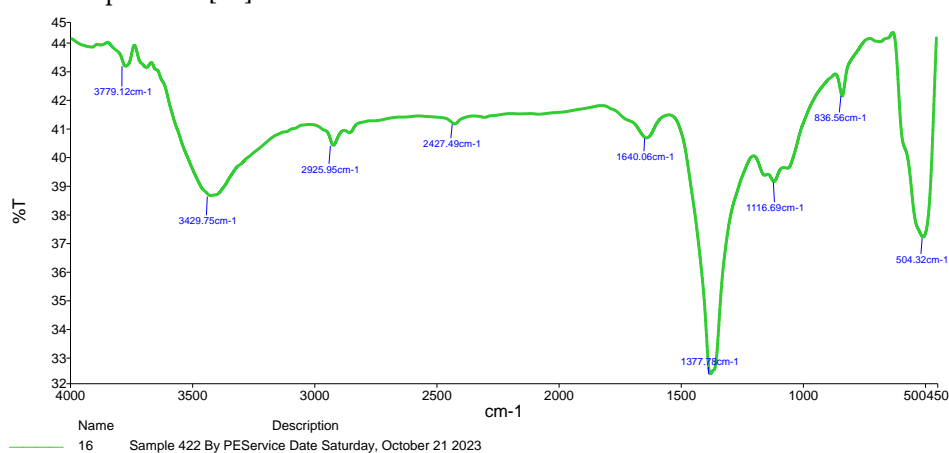


Figure 4. FTIR pattern of *Mentha*-mediated CuO:NiO nanocomposite.

The carbonyl stretching region (1600-1700 cm^{-1}) contains bands that help identify the functional groups of menthol and menthone and other terpenoids which exist in *Mentha* extract [12], [13]. The 1400-1600 cm^{-1} absorption bands originate from aromatic C=C stretching vibrations as well as from C-H bending vibrations of methyl groups. Both CuO and NiO crystalline phases form as indicated by metal-oxygen vibrational modes in the fingerprint region between 500-700 cm^{-1} . The *Cinnamomum cassia*-mediated spectral bands exhibit stronger intensities and modify peak positions which indicates differences in the crystalline nature and particle size dimensions as well as possible changes in Cu ratio [14]. Identical functional groups detected in both samples indicate that phytochemicals including polyphenols and flavonoids as well as other phytochemicals participate in metal ion reduction and nanoparticle encapsulation. The peak diversity in intensity together with placement and form indicates dissimilar molecular interactions which result in various binding mechanisms. Strong absorption bands exist in the aromatic compounds and carbonyl groups spectral regions because *cinnamon* extract contains high levels of both

cinnamaldehyde and eugenol. Potentially significant metal ion reducing compounds make use of their hydroxyl and carbonyl functional groups to perform reduction [15], [16]. The spectral features in the *Mentha*-mediated sample include unique patterns which validate the presence of menthol and menthone along with monoterpenoids. The nanocomposite contains compounds with diverse functional groups that might connect to metal ions using different coordination mechanisms therefore affecting both crystal formation and surface characteristics [17]. The FESEM images show clear variations in the structure of both CuO:NiO nanocomposite created by green synthesis. Fig. 5. FESEM images of (a-left) *Cinnamomum cassia*-mediated nanocomposite mostly have a spherical structure and appear to be accumulating into groups. The particles like to come together in groups and these groups have uneven edges and different sizes.

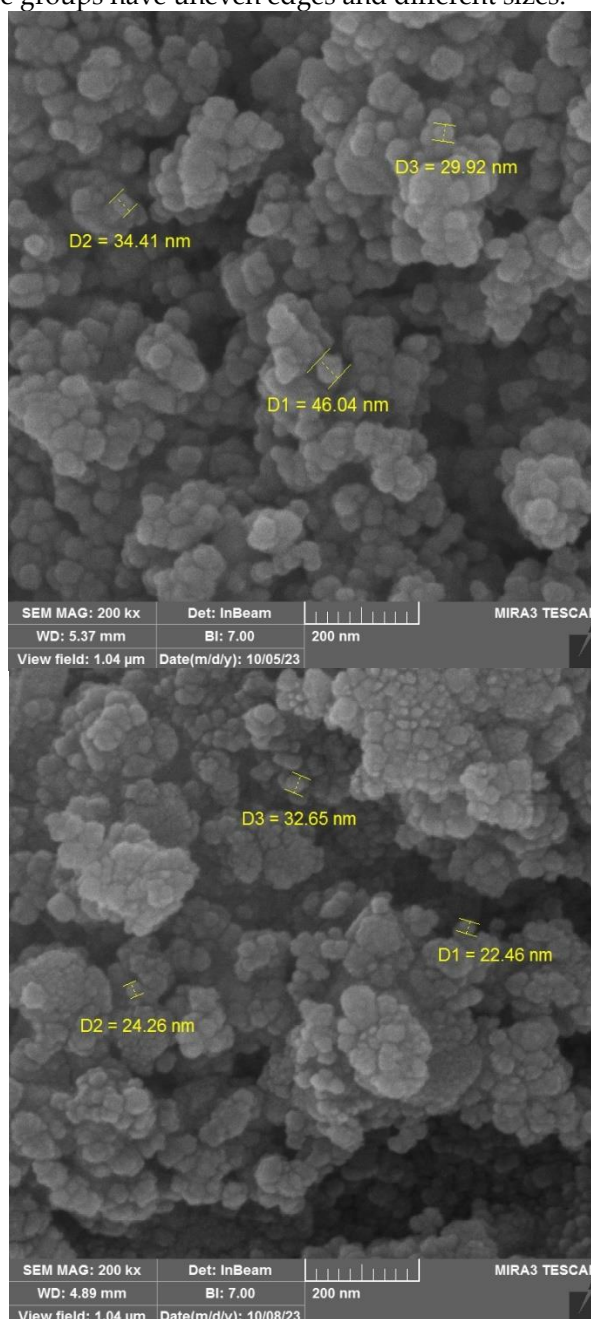


Figure 5. FESEM images of (a-left) *Cinnamomum cassia*-mediated CuO:NiO and (b-right) *Mentha*-mediated CuO:NiO nanocomposites.

The pattern observed here is consistent with what other studies have reported which credit the bridging role of cinnamaldehyde and eugenol during metal oxide nanoparticle synthesis with *cinnamon*. However, Fig. 5. FESEM images of (a-left) show the *Mentha*-

mediated CuO:NiO nanocomposite have a narrower distribution of particle sizes and less agglomeration. Spraying results in individual nanostructures that are well separated from each other. The improved dispersion is thanks to the strong capping action of menthol and flavonoids present in *Mentha*, as they stabilize the nanoparticles and help them avoid widespread aggregation while forming and growing. From the FESEM images and XRD study, it is clear that *Mentha*-mediated nanocomposites have smaller crystallite sizes (20.27 nm) than those formed by using *Cinnamomum cassia* (25.14 nm). By reducing particle size and dispersing them better using *Mentha*, we obtain samples with better surface area-to-volume ratios. This could be useful for activity in catalysis and in biological settings [18], [19]. The morphology of nanoparticles is crucial because it directs their entry into cells, the place they go in the body and the success of their treatment role. While the lower agglomeration in *Mentha*-mediated samples indicates they might reach cells more easily, *Cinnamomum cassia*-mediated samples kill cancer cells more effectively, suggesting other factors are at work. EDX spectrum shown in fig. 6. confirmed the presence of all the elements in both nanomaterials and confirmed that the synthesis of CuO:NiO mixtures was successful. The expected elements found in the *Cinnamomum cassia*-mediated nanocomposite are Cu, Ni and O, with measurements giving Cu (33.69%), Ni (28.00%) and O (35.30%) and some carbon content (3.01%) likely left by plant extract residues [20]. The near 1.2:1 Cu:Ni ratio means that these nanocomposites contain a little more copper than nickel[21].

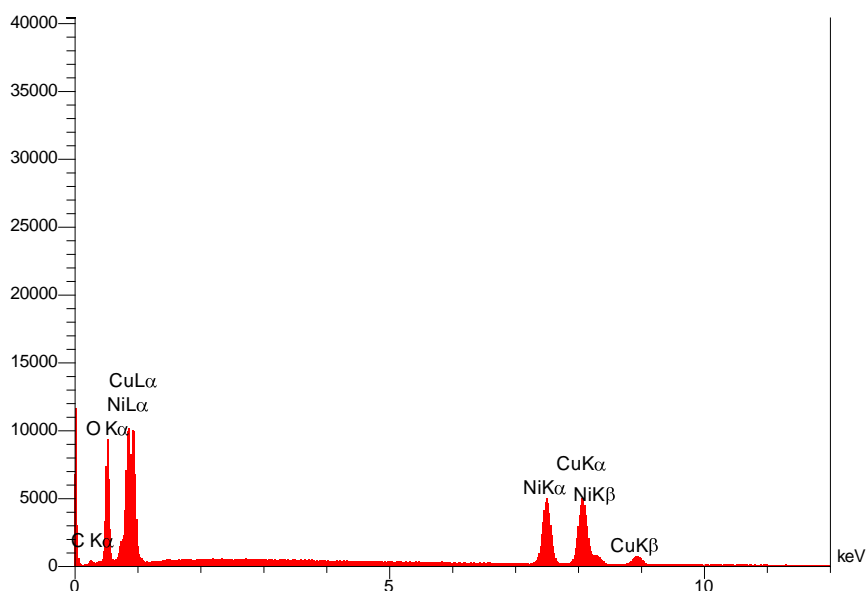


Figure 6. EDX spectrum of *Cinnamomum cassia*-mediated CuO:NiO nanocomposite.

In the EDX spectrum of the *Mentha*-mediated CuO:NiO nanocomposite shown in fig. 6, the element rates are different, with Cu at 21.87%, Ni at 22.10% and O at 34.04%, meaning there is a near-equal amount of Cu and Ni [22]. In addition, it should be noted that this sample carries 16.13% sodium and 3.15% nitrogen, whereas *Cinnamomum cassia*-based samples lack these elements completely. Sodium in the *Mentha*-mediated sample could result from the way *Mentha* extracts and synthesis differ compared to the control [23].(Figure 7)

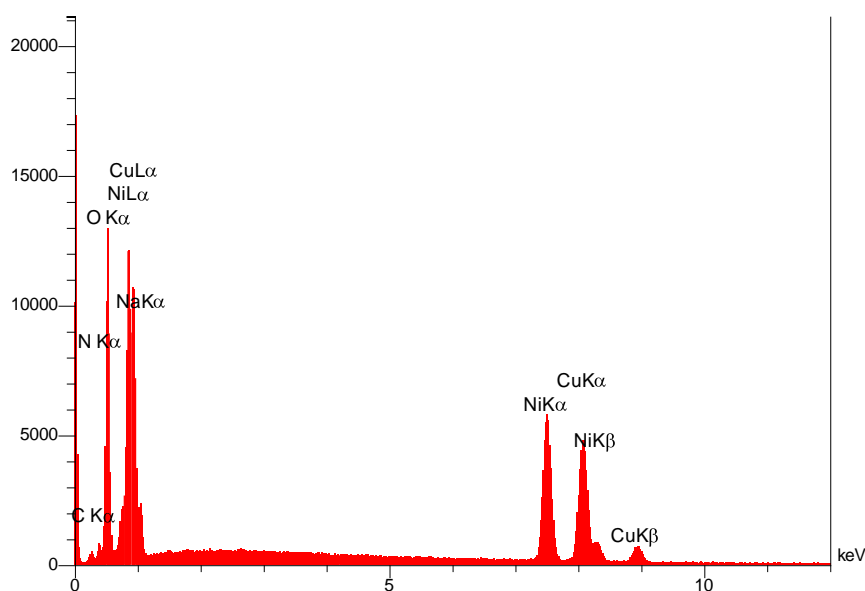


Figure 7. EDX spectrum of *Mentha*-mediated CuO:NiO nanocomposite.

Because both nanocomposites differ greatly in their compositions of elements, their physicochemical features and activities towards cells are influenced mainly by this difference [24]. A greater balance of Cu:Ni in the *Mentha*-mediated sample suggests the same amount of each metal oxide was incorporated uniformly, while the extra metals present in the *Cinnamomum cassia*-mediated sample may give it a slightly higher ability to damage cancer cells [25]. The presence of 35.30% oxygen in *Cinnamomum cassia*-mediated nanocomposites and 34.04% in *Mentha*-mediated ones confirms that metal oxide phases were formed successfully. XRD confirmed that there is CuO and NiO in the final structure, so the presence of oxygen in the sample shows that the process correctly produced these crystalline phases. The presence of oxygen affects both the characteristics and the biological actions of the nanocomposites, since the metal bonds with oxygen help cause oxidative stress to cancer cells. Comparing elemental composition with biological activities revealed that *Cinnamomum cassia*-synthesized nanocomposites had a slightly higher anticancer effect than *Mentha*-synthesized ones. The presence of more metal oxide can promote the production of reactive oxygen species which is thought to lead to cancer cell death.

Cytotoxic effects on DU145 and HFF cells

As presented in Table 1. DU145 cells exhibited concentration-dependent toxicity against both nanocomposites but remained minimally toxic to normal HFF cells. *Cinnamomum cassia*-mediated CuO:NiO nanocomposite demonstrated a decreased viability effect as cells progressed from $100.065 \pm 3.862\%$ at $25 \mu\text{g/mL}$ to $60.273 \pm 13.047\%$ at $800 \mu\text{g/mL}$. The nanocomposites derived from *Mentha* also demonstrated a reduction in DU145 cell viability levels which started at $87.711 \pm 11.5\%$ with $25 \mu\text{g/mL}$ and ended at $58.842 \pm 20.483\%$ with $800 \mu\text{g/mL}$.

Table 1. Cytotoxicity effect of *Cinnamomum cassia*-mediated and *Mentha*-mediated - CuO:NiO nanocomposites on DU145 and HFF cells after 48 hours of incubation at 37°C .

Concentration $\mu\text{g mL}^{-1}$	Mean Viability (%) \pm SD			
	<i>Cinnamomum cassia</i> -mediated - CuO:NiO nanocomposite		<i>Mentha</i> -mediated CuO:NiO nanocomposite	
	DU145	HFF	DU145	HFF
800	60.273 ± 13.047	77.242 ± 9.178	58.842 ± 20.483	82.417 ± 2.753
400	60.013 ± 7.410	79.413 ± 19.373	59.492 ± 25.591	86.007 ± 5.446
200	61.508 ± 20.410	83.222 ± 6.218	71.301 ± 9.556	89.230 ± 3.109
100	61.248 ± 11.030	82.564 ± 10.531	76.723 ± 12.355	88.351 ± 6.658
50	91.937 ± 18.357	85.201 ± 6.396	82.509 ± 4.645	91.648 ± 5.560

25	100.065± 3.862	103.882±25.592	87.711± 11.5	101.758±25.966
----	----------------	----------------	--------------	----------------

The viability levels of normal HFF cells demonstrated significant elevation throughout all tested concentrations. The viability of HFF cells ranged between 103.882±25.592% at 25 µg/mL and 77.242±9.178% at 800 µg/mL in testing *Cinnamomum cassia*-mediated nanocomposites. Effective HFF viability remained between 101.758±25.966% and 82.417±2.753% throughout the entire concentration range of *Mentha*-mediated nanocomposites. The cytotoxic behavior of *Cinnamomum cassia*-mediated and *Mentha*-mediated CuO:NiO nanocomposites varies across Figs. 8 and 9 regarding their influence on the cell lines. (Figure 9)

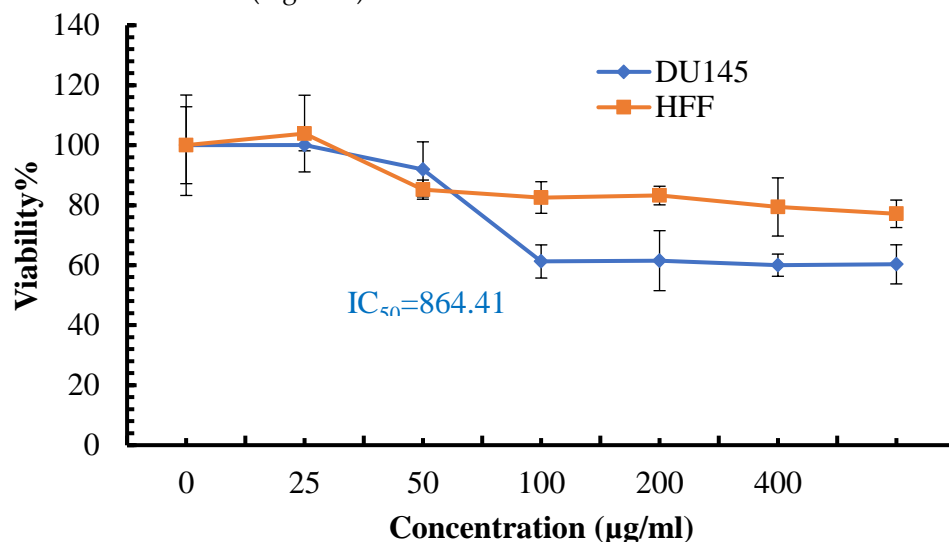


Figure 8. Cytotoxic effect of *Cinnamomum cassia*-mediated -CuO:NiO nanocomposite on DU145 and HFF cells after 48 hrs incubation at 37 °C.

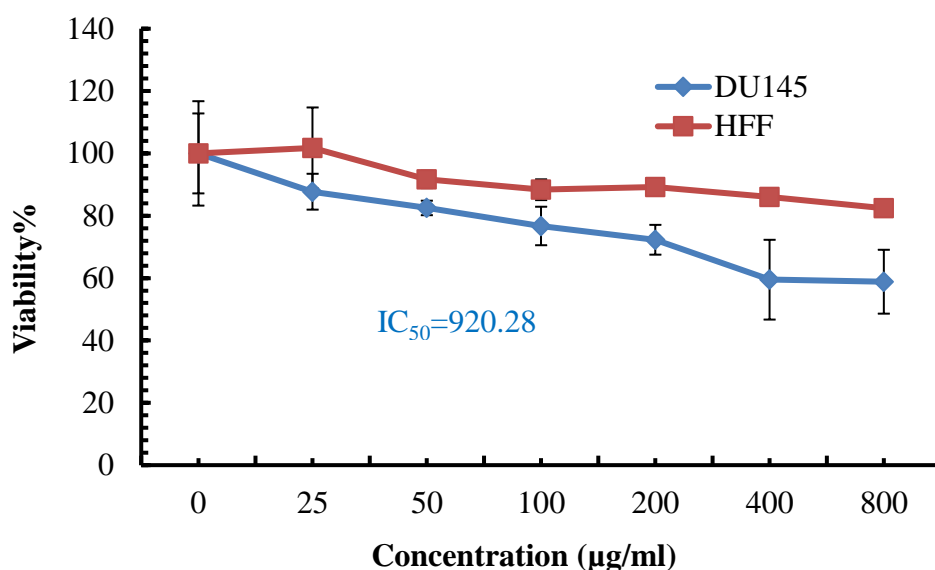


Figure 9. Cytotoxic effect of *Mentha*-mediated - CuO:NiO nanocomposite on DU145 and HFF cells after 48 hrs incubation at 37 °C.

The microscopic analysis of cell death using dose-response curves determined the IC₅₀ value for *Cinnamomum cassia*-mediated to be 864.41 µg/mL while the IC₅₀ value for *Mentha*-mediated nanocomposites became 920.28 µg/mL against DU145 cells thus showing a slight advantage in anticancer activity for the *Cinnamomum cassia*-mediated formulation. The DU145 cellular morphological alterations caused by *Cinnamomum cassia*-mediated and *Mentha*-mediated CuO:NiO nanocomposites at different concentrations appear in Fig. 10. The results presented through the TC₁ and TC₂ columns demonstrate the repeated testing of each concentration while showing the consistency of the obtained results. The

cells showed minimal morphological modifications while being treated with *Cinnamomum cassia* concentrations between 25-50 $\mu\text{g/mL}$ than when compared to DMSO controls. At 100-800 $\mu\text{g/mL}$ the cells displayed a sequence of morphological changes resulting in cell contraction together with membrane abnormality reduced cell numbers and absence of epithelial characteristics [26], [27]. Data showed larger cell alterations in *Cinnamomum cassia*-mediated nanocomposites-treated cells than cells given *Mentha*-mediated nanocomposites at identical concentrations during the time period 400-800 $\mu\text{g/mL}$ (Fig. 10) in accordance with the quantitative viability measures in Table 1. The results were confirmed through combined numerical viability measurements (Table 1) as well as visual inspections (Fig. 10). The selective destruction of cancer cells over normal cells serves as a significant benefit for potential anticancer uses since it deals with the main weakness of standard chemotherapeutic treatments [28]. Multiple factors explain why cancer cells remain more sensitive to cytotoxicity than normal cells during nanoparticle treatments. Oxidative stress from nanoparticle exposure affects cancer cells more than healthy cells because cancer cells maintain altered metabolism with higher levels of reactive oxygen species alongside deficient antioxidant defenses [29]. The enhanced permeability and retention (EPR) effect provides cancer cells with better nanoparticle concentration potential [30]. Cytotoxicity tests show the nanocomposite made from *Cinnamomum cassia* extract ($\text{IC}_{50} = 864.41 \mu\text{g/mL}$) possesses slightly higher interacting potential toward DU145 cells than nanocomposites made from *Mentha* extract ($\text{IC}_{50} = 920.28 \mu\text{g/mL}$).



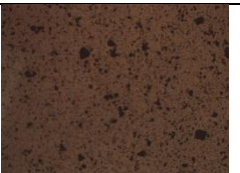

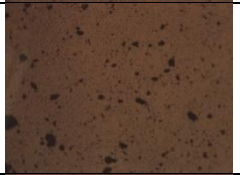
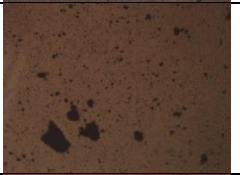
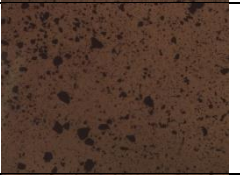
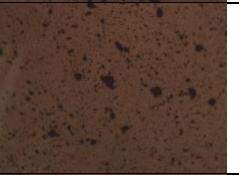
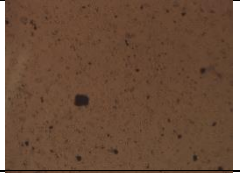


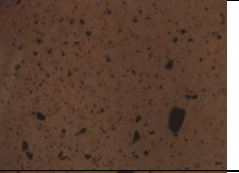




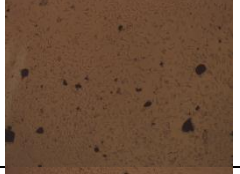







Concentration $\mu\text{g mL}^{-1}$	<i>Cinnamomum cassia</i> -mediated -CuO:NiO nanocomposite		<i>Mentha</i> -mediated nanocomposite CuO:NiO	
	TC ₁	TC ₂	TC ₁	TC ₂
800				
400				
200				
100				
50				
25				



Figure 10. Dose-response curve of DU145 prostate cancer cells treated with *Cinnamomum cassia*-mediated - *Mentha*-mediated CuO:NiO nanocomposites as determined by MTT assay.

This indicates phytochemical elements present in plant extracts can powerfully modulate the biological actions of the final nanocomposite products. The bioactive content of *Cinnamomum cassia* includes cinnamaldehyde and polyphenols together with eugenol which exhibit cell-destroying effects on their own and boost metal oxide nanocomposite toxicity. The biological functions of nanocomposite resulting from *Mentha* species are believed to be shaped by different substances including menthol, rosmarinic acid, and flavonoids according to [31], [32]. Cellular analyses of DU145 cells exposed to nanocomposites revealed modifications that match earlier documented apoptotic patterns in metal oxide nanoparticle research (Fig. 10). The way cells in our experiments shrank along with their density changes preserved patterns known to occur during standard apoptosis [33]. In spite of showing targeted anticancer effects, these nanocomposites must undergo improvements to achieve enhanced therapeutic efficacy since their IC_{50} values exceed 800 $\mu\text{g/mL}$. The therapeutic effects of these nanocomposites can be boosted by contemporary developments in the fields of nanoparticle surface functionalization and both controlled release and targeted delivery systems. When nanocomposites unite with conventional chemotherapeutic agents the effects become synergistic which leads to reduced dosage requirements and lessens the potential toxicity risks [33], [34]. The cytotoxicity of DU145 cells against both nanocomposites showed dose-dependent behavior yet the *Cinnamomum cassia*-mediated nanocomposites exhibited resistance to change in cell viability between 100-800 $\mu\text{g/mL}$ concentrations (Table 1). The observed plateau effect in cellular uptake and adaptive responses underlines the need for investigating nanoparticle-cell interactions at various concentrations.

4. Conclusion

This detailed study reveals that the choice of plant extract greatly changes both the chemical and biological behaviors of CuO:NiO nanocomposites. FESEM observations showed that *Cinnamomum cassia*-tissue nanocomposites had different surfaces, but *Mentha*-tissue composite particles were more uniform and did not agglomerate strongly, as *Mentha* phytochemicals capped them better. The analysis by EDX proved that both methods created CuO:NiO nanocomposites with expected elemental ratios, but the Cu and Ni content differed somewhat in the resulting products. Correlations were found between the atomic and microscopic properties of these compounds and their observed actions against prostate cancer cells. The results revealed that both nanocomposites harmed cancer cells but were nearly harmless to normal HFF cells, making them promising for targeted treatments. It is believed that both cinnamaldehyde and eugenol present in *Cinnamomum cassia* contribute to its slightly better anticancer performance compared to *Mentha*-mediated nanocomposites. Observed changes in form following treatment demonstrate that apoptosis is the main way the cells die. Although selective cytotoxicity has been seen, the low potency calls for improving the effectiveness before further development. Further studies on how to surface-modify, add targeting molecules and complement current anticancer medicines may make these therapies more powerful and still selective. Findings could be applied to health care if researchers study the molecular causes and conduct in vivo experiments. It is found that green synthesis can be used to develop CuO:NiO nanocomposites with potential cancer nanomedicine uses, highlighting the key role of plant-based compounds in shaping nanoparticle qualities and the effects on cancer therapy.

REFERENCES

- [1] Abdal Dayem, M. K. Hossain, S. Bin Lee, K. Kim, S. K. Saha, G.-M. Yang, et al., "The role of reactive oxygen species (ROS) in the biological activities of metallic nanoparticles," *Int. J. Mol. Sci.*, vol. 18, p. 120, 2017.
- [2] P. Khanna, C. Ong, B. H. Bay, and G. H. Baeg, "Nanotoxicity: an interplay of oxidative stress, inflammation and cell death," *Nanomaterials*, vol. 5, pp. 1163–1180, 2015.
- [3] J. K. Patra, G. Das, L. F. Fraceto, E. V. R. Campos, M. del P. Rodriguez-Torres, L. S. Acosta-Torres, et al., "Nano based drug delivery systems: recent developments and future prospects," *J. Nanobiotechnol.*, vol. 16, pp. 1–33, 2018.
- [4] A. M. El Shafey, "Green synthesis of metal and metal oxide nanoparticles from plant leaf extracts and their applications: A review," *Green Process. Synth.*, vol. 9, pp. 304–339, 2020.
- [5] M. Pirsahab, T. Gholami, H. Seifi, E. A. Dawi, E. A. Said, A.-H. M. Hamoody, et al., "Green synthesis of nanomaterials by using plant extracts as reducing and capping agents," *Environ. Sci. Pollut. Res.*, vol. 31, pp. 24768–24787, 2024.
- [6] A. K. Mittal, Y. Chisti, and U. C. Banerjee, "Synthesis of metallic nanoparticles using plant extracts," *Biotechnol. Adv.*, vol. 31, pp. 346–356, 2013.
- [7] C. Zhang, L. Fan, S. Fan, J. Wang, T. Luo, Y. Tang, et al., "Cinnamomum cassia Presl: A review of its traditional uses, phytochemistry, pharmacology and toxicology," *Molecules*, vol. 24, p. 3473, 2019.
- [8] F. Brahmi, M. Khodir, C. Mohamed, and D. Pierre, "Chemical composition and biological activities of Mentha species," in *Aromatic and Medicinal Plants - Back to Nature*, IntechOpen, 2017.
- [9] D. Zhang, C. Jin, H. Tian, Y. Xiong, H. Zhang, P. Qiao, et al., "An in situ TEM study of the surface oxidation of palladium nanocrystals assisted by electron irradiation," *Nanoscale*, vol. 9, pp. 6327–6333, 2017.
- [10] A. Prasad, M. M. Bakr, and A. N. ElMeshad, "Surface-functionalised polymeric nanoparticles for breast cancer treatment: Processes and advances," *J. Drug Target.*, vol. 32, pp. 770–784, 2024.
- [11] B. D. Cullity and R. Smoluchowski, "Elements of X-ray Diffraction," *Phys. Today*, vol. 10, p. 50, 1957.
- [12] A. Monshi, M. R. Foroughi, and M. R. Monshi, "Modified Scherrer equation to estimate more accurately nanocrystallite size using XRD," *World J. Nano Sci. Eng.*, vol. 2, pp. 154–160, 2012.
- [13] V. Selvanathan, M. Shahinuzzaman, S. Selvanathan, D. K. Sarkar, N. Algethami, H. I. Alkhamash, et al., "Phytochemical-assisted green synthesis of nickel oxide nanoparticles," *Catalysts*, vol. 11, p. 1523, 2021.
- [14] R. Sharma, A. Dhillon, and D. Kumar, "Mentha-stabilized silver nanoparticles for high-performance colorimetric detection of Al (III)," *Sci. Rep.*, vol. 8, p. 5189, 2018.
- [15] R. Dash and A. S. Bhattacharyya, "Sequential growth mechanism of Ni-doped CuO nanocrystallites," *MRS Adv.*, vol. 8, pp. 937–942, 2023.
- [16] R. López González, M. H. Gutiérrez, R. L. García, S. A. Gómez Cornelio, C. Lobato, A. Gómez-Rivera, et al., "ZnO nanomaterials with enhanced antimicrobial activity," *J. Chem. Technol. Biotechnol.*, vol. 99, pp. 2535–2544, 2024.
- [17] Y. Li, D. Kong, and H. Wu, "Analysis and evaluation of essential oil components of cinnamon barks using GC–MS and FTIR spectroscopy," *Ind. Crops Prod.*, vol. 41, pp. 269–278, 2013.
- [18] I. Z. Luna, L. N. Hilary, A. M. S. Chowdhury, M. A. Gafur, N. Khan, and R. A. Khan, "Preparation and characterization of copper oxide nanoparticles synthesized via chemical precipitation method," *Open Access Libr. J.*, vol. 2, pp. 1–8, 2015.
- [19] Y. Huang, Y. Liu, H. Tan, Y. Cheng, K. Tao, D. Gu, et al., "Assessing essential oil composition in Cinnamomum cassia leaves using GC-MS and FTIR," *Czech J. Food Sci.*, vol. 42, 2024.
- [20] M. Alavi, S. Dehestaniathar, S. Mohammadi, A. Maleki, and N. Karimi, "Antibacterial activities of phytofabricated ZnO and CuO NPs," *Adv. Pharm. Bull.*, vol. 11, pp. 497–505, 2020.
- [21] O. Taylan, N. Cebi, and O. Sagdic, "Rapid screening of Mentha spicata essential oil and L-menthol in Mentha piperita oil," *Foods*, vol. 10, p. 202, 2021.
- [22] V. V. Makarov, A. J. Love, O. V. Sinitsyna, S. S. Makarova, I. V. Yaminsky, M. E. Taliansky, et al., "Green nanotechnologies: synthesis of metal nanoparticles using plants," *Acta Naturae*, vol. 6, pp. 35–44, 2014.
- [23] A. K. Mittal, Y. Chisti, and U. C. Banerjee, "Synthesis of metallic nanoparticles using plant extracts," *Biotechnol. Adv.*, vol. 31, pp. 346–356, 2013.
- [24] J. K. Patra, G. Das, L. F. Fraceto, E. V. R. Campos, M. del P. Rodriguez-Torres, L. S. Acosta-Torres, et al., "Nano based drug delivery systems: recent developments and future prospects," *J. Nanobiotechnol.*, vol. 16, pp. 1–33, 2018.

- [25] A. M. El Shafey, "Green synthesis of metal and metal oxide nanoparticles from plant leaf extracts," *Green Process. Synth.*, vol. 9, pp. 304–339, 2020.
- [26] F. Brahmi, M. Khodir, C. Mohamed, and D. Pierre, "Biological activities of *Mentha* species," in *Aromatic and Medicinal Plants*, IntechOpen, 2017.
- [27] Y. Huang, Y. Liu, H. Tan, Y. Cheng, K. Tao, D. Gu, et al., "Essential oil composition in *Cinnamomum cassia* leaves," *Czech J. Food Sci.*, vol. 42, 2024.
- [28] D. Zhang, C. Jin, H. Tian, Y. Xiong, H. Zhang, P. Qiao, et al., "Surface oxidation of palladium nanocrystals," *Nanoscale*, vol. 9, pp. 6327–6333, 2017.
- [29] R. Sharma, A. Dhillon, and D. Kumar, "Colorimetric detection of Al (III) with silver nanoparticles," *Sci. Rep.*, vol. 8, p. 5189, 2018.
- [30] R. Dash and A. S. Bhattacharyya, "Ni-doped CuO nanocrystallites growth mechanism," *MRS Adv.*, vol. 8, pp. 937–942, 2023.
- [31] R. López González, M. H. Gutiérrez, R. L. García, S. A. Gómez Cornelio, C. Lobato, A. Gómez-Rivera, et al., "ZnO nanomaterials via *Eichhornia crassipes*," *J. Chem. Technol. Biotechnol.*, vol. 99, pp. 2535–2544, 2024.
- [32] M. Alavi, S. Dehestaniathar, S. Mohammadi, A. Maleki, and N. Karimi, "Phytofabricated ZnO and CuO NPs antibacterial activity," *Adv. Pharm. Bull.*, vol. 11, pp. 497–505, 2020.
- [33] O. Taylan, N. Cebi, and O. Sagdic, "ATR-FTIR spectroscopy of *Mentha* oils," *Foods*, vol. 10, p. 202, 2021.
- [34] V. V. Makarov, A. J. Love, O. V. Sinitsyna, S. S. Makarova, I. V. Yaminsky, M. E. Talianky, et al., "Synthesis of metal nanoparticles using plants," *Acta Naturae*, vol. 6, pp. 35–44, 2014.